



# Znf469 Plays a Critical Role in Regulating Synthesis of ECM: A Zebrafish Model of Brittle Cornea Syndrome

Jing Bao,<sup>1,2</sup> Xiaoning Yu,<sup>1,2</sup> Xiyuan Ping,<sup>1,2</sup> Xingchao Shentu<sup>1,2</sup> , and Jian Zou<sup>1-3</sup> 

<sup>1</sup>Eye Center, The Second Affiliated Hospital, Zhejiang University School of Medicine, Hangzhou, Zhejiang, China

<sup>2</sup>Zhejiang Provincial Key Lab of Ophthalmology, Hangzhou, Zhejiang, China

<sup>3</sup>The Institute of Translational Medicine, Zhejiang University, Hangzhou, Zhejiang, China

Correspondence: Jian Zou, The Institute of Translational Medicine, Zhejiang University, 268 Kaixuan Road, Shangcheng District, Hangzhou, Zhejiang 310029, China; [jianzou@zju.edu.cn](mailto:jianzou@zju.edu.cn).

Xingchao Shentu, Eye Center, The Second Affiliated Hospital, Zhejiang University School of Medicine, 88 Jiefang Road, Shangcheng District, Hangzhou, Zhejiang 310009, China; [stxc@zju.edu.cn](mailto:stxc@zju.edu.cn).

JB and XY contributed equally to the work presented here and should therefore be regarded as equivalent authors.

**Received:** November 6, 2022

**Accepted:** May 11, 2023

**Published:** May 31, 2023

Citation: Bao J, Yu X, Ping X, Shentu X, Zou J. *Znf469* plays a critical role in regulating synthesis of ECM: A zebrafish model of brittle cornea syndrome. *Invest Ophthalmol Vis Sci.* 2023;64(5):29. <https://doi.org/10.1167/iovs.64.5.29>

**PURPOSE.** Brittle cornea syndrome (BCS) is a rare autosomal recessive disorder characterized by extreme thinning and fragility of the cornea, and mutations in *ZNF469* cause BCS-1. We aimed to establish a *znf469* mutant zebrafish line to explore its roles and possible pathogenic mechanism in cornea development and disorder.

**METHODS.** *znf469*<sup>idel/4del</sup> mutant zebrafish was generated using the CRISPR/Cas9 technology. Transmission electron microscopy (TEM) was performed to examine the phenotype of the cornea in different developmental stages. RNA sequencing and quantitative real-time polymerase chain reaction were used to reveal the molecular mechanism.

**RESULTS.** Macroscopically, homozygous *znf469* mutant zebrafish larvae exhibited a curved body from 72 hours postfertilization, similar to kyphoscoliosis, and a noninflated swim-bladder at 7 days postfertilization (dpf). TEM revealed an extreme reduction of corneal stroma thickness in homozygous *znf469* mutant zebrafish in both the central and peripheral cornea from the early development stage. RNA-sequencing analysis demonstrated that the *znf469* mutation leads to the decreased synthesis of various extracellular matrix (ECM) components, such as collagens and proteoglycans, but increased synthesis of 26S proteasome family members.

**CONCLUSIONS.** The results of our work indicate that *znf469* is a critical gene that, as a widely considered transcription factor, may regulate the synthesis and degradation of a large number of ECM components that play an important role in corneal development.

**Keywords:** BCS, *ZNF469*, *znf469*, zebrafish model, CRISPR/Cas9, ECM, RNA-seq

Brittle cornea syndrome (BCS) is a rare autosomal recessive disorder characterized by extreme thinning and fragility of the cornea, with keratoconus (KC) and blue sclera as major ocular manifestations. Other ocular signs include keratoglobus, high myopia, irregular corneal astigmatism, and corneal rupture.<sup>1</sup> Disorder of collagen-rich extracellular matrix (ECM) synthesis and homeostasis is the major cause of BCS. BCS is genetically heterogeneous and caused by biallelic mutations in either *ZNF469* (BCS-1, OMIM 22920) or *PRDM5* (BCS-2, OMIM 614170).<sup>2</sup>

*ZNF469* belongs to the Cys2-His2 (C2H2) zinc finger family, which is considered to encode a class of transcription factors.<sup>3</sup> Genome-wide association studies have repeatedly indicated that *ZNF469* is strongly associated with central corneal thickness.<sup>4-10</sup> Mounting evidence has shown that *ZNF469* heterozygous missense mutations are associated with a keratoconic phenotype,<sup>11-13</sup> which indicates autosomal dominant inheritance. Conversely, several groups found no association between mutations in *ZNF469* and KC,<sup>14,15</sup> suggesting a complicated pathogenic mechanism of *ZNF469* mutations. Furthermore, *ZNF469* is reported to be a pathogenic gene of systemic connective tissue disease in humans.<sup>16</sup> Current evidence suggests that *ZNF469* may play

a role in collagen biosynthesis and assembly<sup>17</sup> and regulation of ECM homeostasis.<sup>16</sup>

A recent study in a mouse model reported that homozygous *Zfp469* mutant mice weigh less but are viable and fertile. Depletion of *Zfp469* in mice induces decreased expression of ECM components, especially *Col1a1* and *Col1a2*, but not *Col5a1*. The abnormal collagen type I/collagen type V ratio may result in collagen fibrils with smaller diameter and increased fibril density. As a result, the corneal stroma thickness of homozygous mutants is reduced by approximately 50% after conversion according to the thickness ratio of the epithelium and stroma.<sup>18</sup> In this study, we generated a *znf469* mutant zebrafish line to elucidate its roles in zebrafish corneal development and applied RNA-sequencing (RNA-seq) to elucidate the possible pathogenesis of BCS induced by *znf469* mutations.

## MATERIALS AND METHODS

### Patient

In our previous research, seven novel mutations in *ZNF469* were identified and predicted to have a pathogenic role in

Chinese patients with KC.<sup>12</sup> Here, we evaluated a patient with severe ocular signs. The patient was a 30-year-old man. He underwent a corneal topography that used an Oculus Pentacam 1.21r41 (Oculus Optikgeräte GmbH, Wetzlar, Germany). Genomic DNA extracted from a blood sample using a Simgen Blood DNA mini kit (Simgen, Hangzhou, China) was applied to screen the mutations with next-generation sequencing technology, which is based on targeted sequence capturing technology with the SureSelect Target Enrichment Kit (Agilent Technologies, Santa Clara, CA, USA) and Illumina sequencing technology using a HiSeq sequencer (Illumina, San Diego, CA, USA). To avoid false-positive results and to ascertain the significance of the mutations in *ZNF469*, mutations with a minor allele frequency < 0.1% (according to data from the May 2012 release of the 1000 Genomes Project and the Single Nucleotide Polymorphism database) and absent from the results of the whole-exome sequencing data acquired from 220 Han Chinese individuals without ocular abnormalities (from a commercial database provided by the Genesky Bio-Tech company) were subsequently confirmed using Sanger sequencing technology. Written informed consent was obtained.

### Zebrafish Husbandry

All experiments, including the generation of mutants, were conducted on AB strain zebrafish. The zebrafish were maintained at 27.5°C ± 1°C with a 14-hour light/10-hour dark photoperiod. Embryos were collected and maintained in E3 medium in a 28.5°C incubator. Animal care and experimental procedures were approved by the Ethics Committee on Animal Research of Zhejiang University. All procedures conformed to the protocols of the Zhejiang University Animal Care and Use Committee.

### Generation of *znf469* Loss-of-Function Zebrafish Line and Genotyping

Clustered regularly interspaced short palindromic repeats/Cas9 (CRISPR/Cas9) technology was applied to generate *znf469* mutants following previously described protocols.<sup>19</sup> The specific guide RNA (gRNA) sequence targeting the c.495-514 region in the single coding exon of the *znf469* gene (Fig. 2B), 5'-GAATACTTGGCACATGGAAG-3', was designed by a website (<http://crispor.tefor.net>) and synthesized using the MEGAscript T7 kit (AM1334; Thermo Fisher Scientific, Waltham, MA, USA). The mixtures (approximately 4 nL), including 800 ng/μL NLS-Cas9-NLS protein (Z03389; GenScript, Piscataway, NJ, USA) and 200 ng/μL single-guide RNA (sgRNA) were coinjected into one-cell zygote embryos. The founders (F0) were raised and outcrossed with wild-type (WT) fish to obtain F1 fish. The adult F1 fish were genotyped by Sanger sequencing (Fig. 2C). A 4-base pair (bp) deletion strain was detected and outcrossed with WT until F3. The mutation introduced a recognition site of NspI. The 4-bp deletion strain was genotyped by PCR and digestion with restriction enzyme NspI (R0602S; New England Biolabs, Ipswich, MA, USA) (Fig. 2E). The genotyping PCR primers were as follows:

F: 5'-CAAACCAACGCTCAAATCCCAC-3'  
R: 5'-CCTCTCTGAAGAGTGCCATGTGT-3'

### Transmission Electron Microscopy

Zebrafish larvae at the desired developmental stage were fixed overnight at 4°C in 2.5% glutaraldehyde plus 2%

paraformaldehyde in 0.1-M PBS. After three 15-minute washes in PBS (0.1-M, pH 7.0), larvae were postfixed with 1% SPI-Chem osmium tetroxide (02595-BA; Structure Probe, Inc., West Chester, PA, USA) for 1 hour and then washed of osmium using PBS three times, 15 minutes each. Next, the larvae were dehydrated by a graded series of ethanol (30%, 50%, 70%, 80%) and acetone (90%, 95%) for 15 minutes each. Finally, the sections were dehydrated twice for 20 minutes in absolute acetone. The larvae were placed in a 1:1 mixture of absolute acetone and the final Spurr resin (02680-AB; Structure Probe, Inc.) mixture for 1 hour at room temperature. They were then transferred to a 1:3 mixture of absolute acetone and the final resin mixture for 3 hours and to the final Spurr resin mixture overnight. Larvae were placed in an Eppendorf tube containing Spurr resin, heated at 70°C for more than 9 hours, and then sectioned in a Leica EM UC7 ultratome (Leica, Wetzlar, Germany). Every effort was made to achieve sagittal sections at the equator of the eyes. Sections were with by uranyl acetate and alkaline lead citrate for 5 to 10 minutes and observed with a Hitachi H-7650 transmission electron microscope (Hitachi, Tokyo, Japan).

### RNA-Seq and Bioinformatics Analysis

Total RNA was isolated from a pool of 50 homozygous mutant or WT larvae at 7 days postfertilization (dpf). RNA-seq and analysis were performed at RiboBio (Guangzhou, China). The quality of the RNA libraries was assessed using the Agilent 2200 TapeStation (Agilent Technologies, Santa Clara, CA, USA), and libraries were sequenced by the Illumina platform with paired-end 150 bp. Clean reads were aligned to the zebrafish reference genome sequence (GRCz11) using HISAT2 2.1.0 with default parameters. HTSeq 0.12.4 was subsequently employed to convert aligned short reads into read counts for each gene model. Differential expression was assessed by DESeq2 using read counts as input. The Benjamini-Hochberg multiple test correction method was enabled. Differentially expressed genes (DEGs) were chosen according to the criteria of  $|\log_2\text{FoldChange}| > 1$  and adjusted  $P(Q) < 0.05$ . The clusterProfiler 3.12.0 package in R/Bioconductor (R Foundation for Statistical Computing, Vienna, Austria)/KOBAS 3.0 was used to identify and visualize the GO terms and Kyoto Encyclopedia of Genes and Genomes (KEGG) pathways enriched by all DEGs.

### Quantitative Real-Time PCR Analysis

Total RNA was isolated from a pool of five homozygous mutants and heterozygous or WT larvae at 7 dpf using TRIzol (15596026; Thermo Fisher Scientific). RNA samples were reverse transcribed using the PrimeScript RT reagent kit (RR047A; Takara Bio, Shiga, Japan). Two-step quantitative real-time PCR (qRT-PCR) was then performed using PowerUp SYBR Green Master Mix (A25742; Thermo Fisher Scientific) on a CFX96 Real-Time PCR System (Bio-Rad, Hercules, CA, USA). Data are represented as the mean ± SD of three independent biological replicates. The *actb1* gene that encodes  $\beta$ -actin1 was used as an internal control. Data were analyzed using the  $2^{-\Delta\Delta CT}$  method for relative quantitation. All of the primers are listed in Supplementary Table S1.

### Data Analysis

The measurements of the thickness of corneal layers (total, epithelium, stroma, and endothelium) were performed on five transmission electron microscopy (TEM) digital

micrographs taken of both the central and peripheral cornea using ImageJ 1.53 (National Institutes of Health, Bethesda, MD, USA). Quantitative data are shown as the means  $\pm$  SD. Unpaired Student's *t*-test was used to compare the means from two different groups, and one-way ANOVA with multiple comparisons was used to compare the means from three or more groups using Prism 9 9.1.1 (GraphPad, San Diego, CA, USA).  $P < 0.05$  was considered significant.

## RESULTS

### Keratoconus and Global Corneal Thinning in a Patient With a *ZNF469* Mutation

The index patient described here presented with corneal stromal thinning, Vogt's striae, Fleischer ring, and Munson's sign in both eyes under the slit-lamp microscope, and his corneal topography analysis revealed reduced corneal thickness and increased corneal central curvature, and the thinnest point of the cornea had moved downward (Fig. 1), which met the diagnostic criteria for KC. Genomic DNA sequencing revealed that the patient carried a heterozygous missense variant in *ZNF469* (c.3749C>T), leading to the amino acid substitution P1250L. Unknown significance was assigned to the *ZNF469* (c.3749C>T;p.P1250L) variant according to the American College of Medical Genetics and Genomics/Association for Molecular Pathology 2015 classification guidelines. Silico analysis with the Sorting Intolerant Form Tolerant (SIFT) program predicted the variant as a damaging mutation. Previous studies suggest that biallelic mutations in *ZNF469* cause BCS, whereas heterozygous carriers of the pathogenic variant tend to show mild or no corneal thinning.<sup>14,17</sup> Considering that patients with BCS typically present with an autosomal-recessive general-

ized connective tissue disorder (such as the abnormalities in corneal, skin, auditory, and musculoskeletal tissue), the index patient did not meet the diagnostic criteria for BCS because he did not show any other clinical manifestations except KC and did not fit the normal recessive inheritance for the disease. In a word, this case supports the observation that heterozygous carriers of *ZNF469* mutations lead to KC.

### Generation of *znf469* Mutant Zebrafish and Identification of Macroscopic Phenotype

The seven predicted C2H2 zinc finger domains of the *Znf469* protein (XP\_021326388.1) showed extremely high conservation compared to the human *ZNF469* protein (NP\_001354553.1) (Fig. 2A). Zebrafish *znf469* contains a single coding exon with a coding sequence (CDS) of 11,253 bp. The CRISPR target site was designed in the CDS c.495-514 region (Fig. 2B). Sanger sequencing results revealed a 4-bp deletion in the homozygous *znf469* mutant zebrafish (c.496-499del, p.Phe166Metfs\*43), which introduced a recognition site of the restriction enzyme *NspI*. We refer to the *znf469* mutant line as *znf469*<sup>4del/4del</sup> (Fig. 2C). The 4-bp deletion is expected to cause a frameshift and generate a premature stop codon, leading to early termination of protein translation and a truncated *Znf469* protein with 208 amino acids leading to the loss of all of the zinc finger domains in *znf469*<sup>4del/4del</sup> zebrafish (Fig. 2D). PCR products amplified from extracted genomic DNA followed by *NspI* digestion were carried out to distinguish the homozygous mutants (Fig. 2E). No significant difference was observed for the expression levels of *znf469* mRNA among heterozygous and homozygous mutation carriers and WT larvae, indicating that the mutant

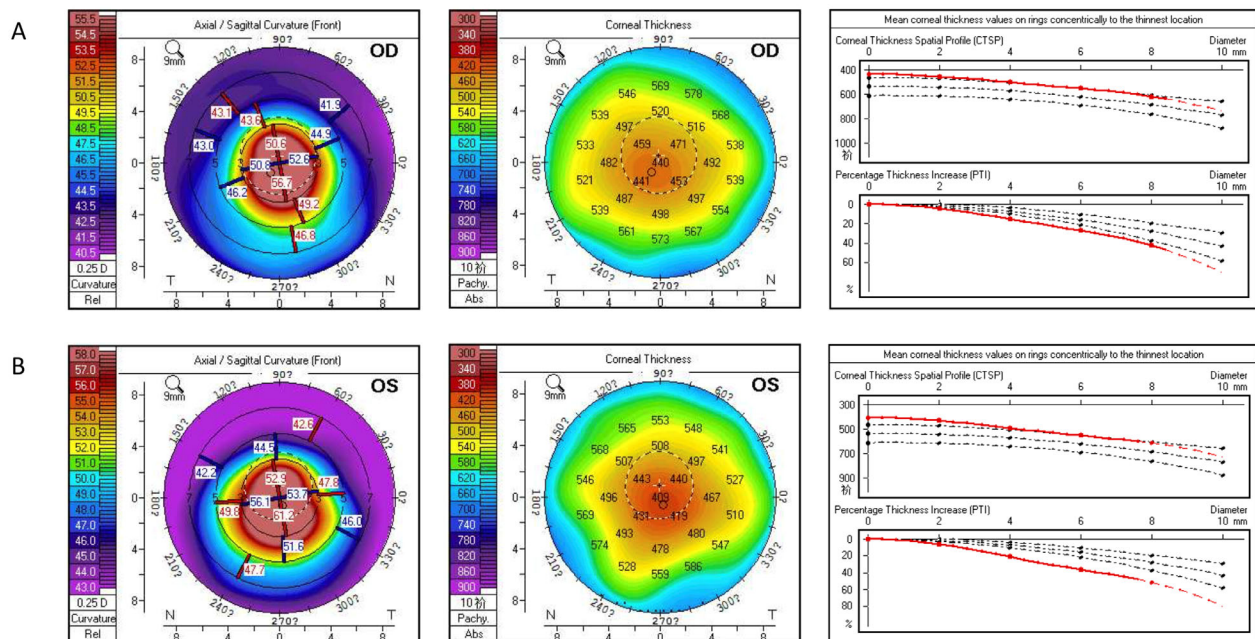


**FIGURE 1.** Clinical ocular features of the *ZNF469* mutant patient. **(A)** Pentacam refractive maps and corneal thickness map of the right eye (OD). Thinnest corneal thickness = 435  $\mu$ m,  $K_{max}$  = 64.9 D. **(B)** Pentacam refractive maps and corneal thickness map of the left eye (OS). Thinnest corneal thickness = 406  $\mu$ m,  $K_{max}$  = 70.4 D. Pupil center is indicated by a plus sign (+), the pachy apex is marked with a filled circle ( $\bullet$ ), and the thinnest location is indicated by an open circle ( $\circ$ ). Three black dotted lines in the corneal thickness map indicate the distribution of healthy people, and the red line indicates the fitting curve of the patient.

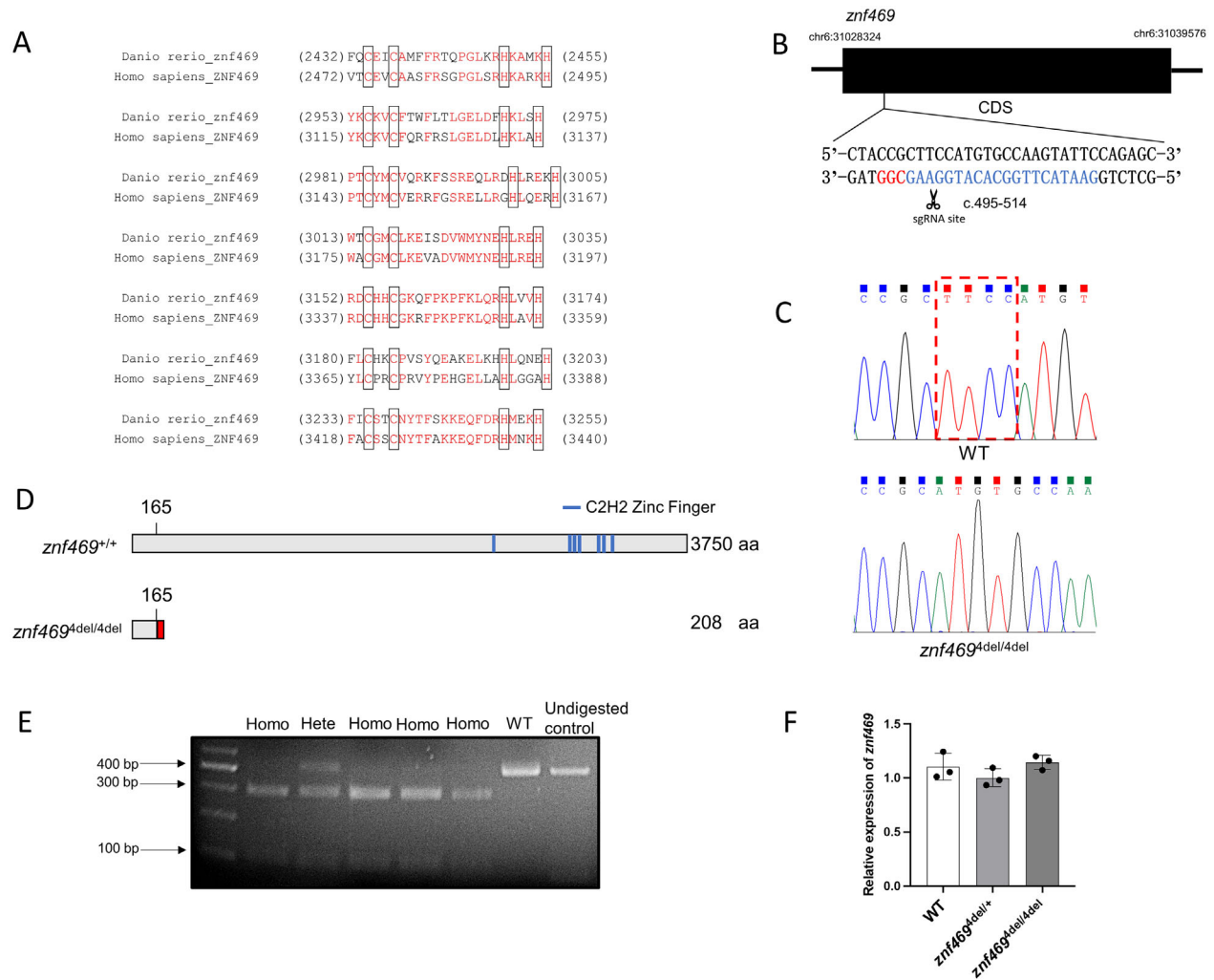


**FIGURE 2.** Generation of *znf469* mutant zebrafish. **(A)** Sequence alignment of the seven C2H2 zinc finger protein domains in zebrafish *Znf469* protein and human *ZNF469* protein. The identical residues are colored in *red*. Residues shown in the *black box* are the paired cysteines and histidines, which bind the zinc ion. **(B)** Schematic diagram of the zebrafish *znf469* gene CDS region. The single-guide RNA (sgRNA) targeting site is marked in *blue*, and the protospacer adjacent motif (PAM) sequence adjacent motif (PAM) sequence is marked in *red*. **(C)** Sanger sequencing results revealed a 4-bp deletion (c.496-499del) in the *znf469* homozygous mutant zebrafish. **(D)** Schematic representation of the protein structure of *Znf469* and the position of the seven predicted C2H2 zinc finger domains. The 4-bp deletion caused a frameshift; the 166th and subsequent amino acids began to change (marked with *red segment*) and then generated a premature stop codon, leading to early termination of protein translation and a truncated *Znf469* protein with 208 amino acids in *znf469*<sup>4del/4del</sup> zebrafish. **(E)** The mutant zebrafish were genotyped with PCR, followed by *NspI* digestion. The undigested WT PCR product was loaded as a control. The mutant allele could be digested into two fragments for the addition of the *NspI* digestion site, but the WT allele could not be digested. **(F)** qRT-PCR analysis revealed no significant difference in the level of *znf469* mRNA in the WT, *znf469*<sup>4del/+</sup>, and *znf469*<sup>4del/4del</sup> larvae at 7 dpf. Three biological replicates were performed, and the data are shown as the mean  $\pm$  SD.



**FIGURE 3.** Macroscopic phenotype of the *znf469* mutant zebrafish. **(A)** The larvae of *znf469*<sup>4del/4del</sup> zebrafish had slightly curved bodies compared to the WT larvae at 72 hpf. The larvae of *znf469*<sup>4del/+</sup> zebrafish showed no phenotypic abnormalities. **(B)** The larvae of *znf469*<sup>4del/4del</sup> zebrafish lacked an inflated swimbladder (indicated by a *red asterisk*, \*) and had a curved body compared to WT larvae at 7 dpf. The larvae of *znf469*<sup>4del/+</sup> zebrafish showed no phenotypic abnormalities.

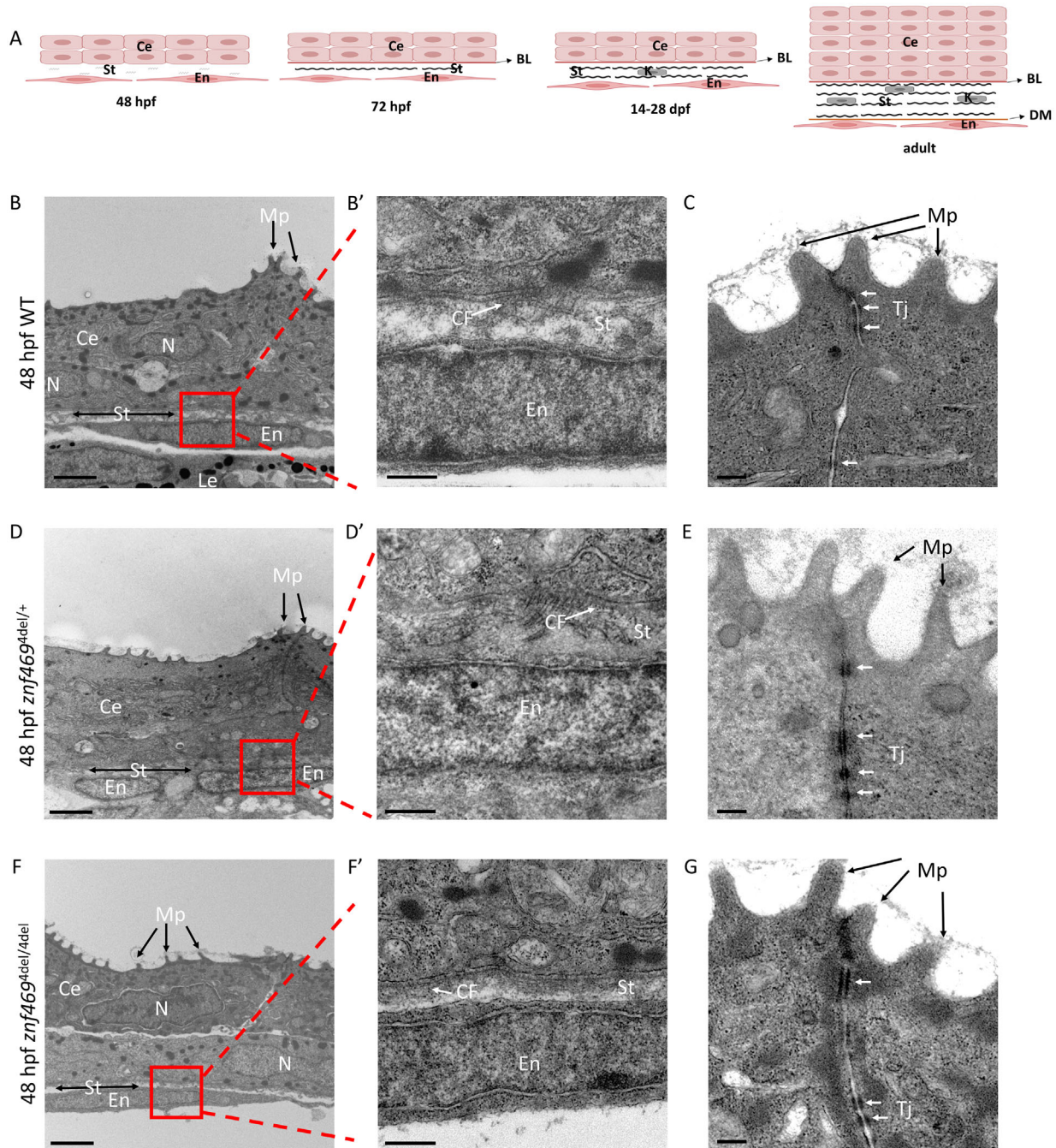


**FIGURE 4.** Similar ultrastructure of cornea in WT, *znf469*<sup>4del/+</sup>, and *znf469*<sup>4del/4del</sup> zebrafish larvae at 48 hpf. (A) Schematic diagram of zebrafish corneal development. To adulthood, the epithelium increases to four to six layers, the stroma is thickened, the density of keratocytes is increased, Descemet's membrane is visible, and the endothelium is also a monolayer. The TEM ultrastructure of the cornea is shown in WT (B, B', C), *znf469*<sup>4del/+</sup> (D, D', E), and *znf469*<sup>4del/4del</sup> (F, F', G) zebrafish larvae at 48 hpf. Each cornea contains a bilayer epithelium, a primary stroma, and a monolayer endothelium. Collagen fibers are visible but not well organized. B, D, and F show the cornea at low magnification. B', D', and F' are the enlarged images of the primary stroma showed in the red boxes in B, D, and F, respectively; C, E, and G show the intercellular junctions between the superficial layer of the epithelium. Mp, microplacae; Ce, corneal epithelium; N, nucleus; St, stroma; En, endothelium; Le, lens epithelium; CF, collagen fiber; Tj, tight junction; BL, Bowman's layer; K, keratocyte; DM, Descemet's membrane. Scale bars: 2  $\mu$ m (B, D, F); 500 nm (B', D', F'); 200 nm (C, E, G).

transcripts did not undergo nonsense-mediated decay (Fig. 2F).

The larvae of *znf469*<sup>4del/4del</sup> zebrafish had slightly curved bodies compared to WT larvae at 72 hours postfertilization (hpf), whereas the *znf469*<sup>4del/+</sup> zebrafish seemed

to be unaffected (Fig. 3A). The homozygous mutation of *znf469* compromised viability from 7 dpf on due to the curved body and the absence of an inflated swimbladder (Fig. 3B, marked with red \*). Homozygous mutant larvae sank to the bottom and were unable to actively swim,

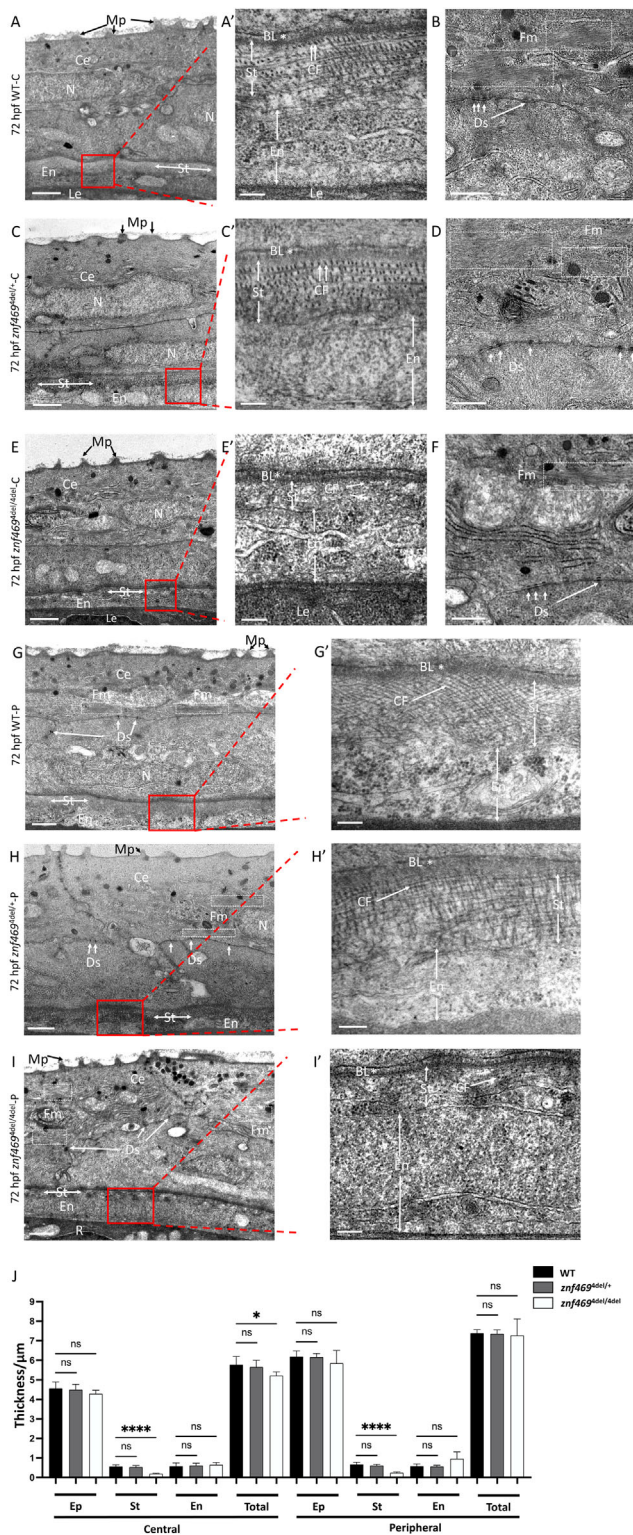


**FIGURE 5.** *znf469* homozygous mutation in zebrafish results in a significant reduction of corneal stroma thickness at 72 hpf. The TEM ultrastructure of the cornea is shown in WT (A, A', B, G, G'), *znf469*<sup>4del/+</sup> (C, C', D, H, H'), and *znf469*<sup>4del/4del</sup> (E, E', F, I, I') zebrafish larvae. The stroma components decreased significantly and the collagen fibers were few and disorderly arranged in *znf469*<sup>4del/4del</sup> mutant zebrafish at 72 hpf compared to WT zebrafish. A, C, and E show the central cornea at low magnification. G, H, and I show the peripheral cornea at low magnification. A', C', E', G', H', and I' are the enlarged images of the primary stroma shown in the red boxes in A, C, E, G, H, and I, respectively. B, D, and

and they eventually died at 7 to 10 dpf. The larvae of *znf469*<sup>4del/+</sup> zebrafish showed no apparent macroscopic abnormalities. *Znf469*<sup>4del/+</sup> adult zebrafish were viable and fertile.

### *znf469*<sup>4del/4del</sup> Mutation Results in an Extreme Reduction of Primary Stroma in Whole Cornea

The adult zebrafish cornea has five layers similar to humans: epithelium, Bowman's layer, stroma, Descemet's membrane and endothelium. The development of zebrafish cornea occurs in several stages.<sup>20–22</sup> The corneal epithelial cells separate from the lens epithelial cells at 24 hpf. The stroma starts to accumulate on the internal surface of the corneal epithelium at 30 hpf. By 48 hpf, endothelial cells form a monolayer, separated from the epithelial cells by a robust stroma. At 72 hpf, the cornea contains two layers of epithelial cells: the well-organized primary stroma and a single cell layer of the endothelium. From 14 to 28 dpf, the stroma increases rapidly, and keratocytes appear in the stroma (Fig. 4A). To investigate the roles of *znf469* in corneal development, we analyzed the phenotypes of WT, *znf469*<sup>4del/+</sup>, and *znf469*<sup>4del/4del</sup> zebrafish larvae at 48 hpf, 72 hpf, and 7 dpf using TEM.

For WT larvae at 48 hpf, the corneal epithelium had two cell layers, and the superficialities formed numerous microplacae (Figs. 4B, 4C). The acellular stromal rudiment was still loose and not well organized, and some collagen fibers can be seen in the enlarged photograph (Figs. 4B, 4B'). Endothelial cells had completed their migration from the periphery to form a monolayer of endothelium (Figs. 4B, 4B'). Tight junctions were observed between the adjacent cells of the superficial layer of the epithelium (Fig. 4C). For *znf469*<sup>4del/+</sup> (Figs. 4D, 4D', 4E) and *znf469*<sup>4del/4del</sup> (Figs. 4F, 4F', 4G) larvae at 48 hpf, the shape and structure of the cornea were similar to those of the WT larvae, suggesting that the migration and organization of the corneal epithelium and endothelium were not affected.

For WT larvae at 72 hpf, there were two layers of epithelial cells and one layer of endothelial cells in both the central cornea (Fig. 5A) and the peripheral cornea (Fig. 5G). From 48 hpf to 72 hpf, one major change was that the primary corneal stroma developed rapidly. At 72 hpf, the thickness of the stroma increased significantly, and the collagen fibers had formed a well-organized, orthogonal, and multilayer structure (Figs. 5A, 5A', 5G, 5G'). The other major change was that some important structures began to appear, such as the desmosomes between the adjacent cells of the two epithelial layers: the fibril-like structure in the superficial epithelium (Figs. 5B, 5G) and Bowman's layer (Figs. 5A', 5G'). For *znf469*<sup>4del/4del</sup> zebrafish at 72 hpf, the thickness of the stroma

F show that Fibril-like materials and cell junctions (desmosomes) can be observed in *znf469*<sup>4del/+</sup> and *znf469*<sup>4del/4del</sup> zebrafish at 72 hpf, with no significant difference compared to WT zebrafish. J shows the thickness of each layer in the total, central, and peripheral cornea in WT, *znf469*<sup>4del/+</sup>, and *znf469*<sup>4del/4del</sup> zebrafish at 72 hpf. The thickness of the central and peripheral corneal stroma is significantly reduced in *znf469*<sup>4del/4del</sup> mutant zebrafish ( $n = 5$  for each genotype; data are shown as the mean  $\pm$  SD; \* $P < 0.05$ , \*\*\*\* $P < 0.0001$ ). Mp, microplacae; Ce, corneal epithelium; N, nucleus; St, stroma; En, endothelium; Le, lens epithelium; R, retina; BL, Bowman's layer; CF, collagen fiber; Fm, fibril-like material; Ds, desmosome. Scale bars: 1  $\mu$ m (A, C, E, G, H, I); 200 nm (A', C', E', G', H', I'); 500 nm (B, D, F).

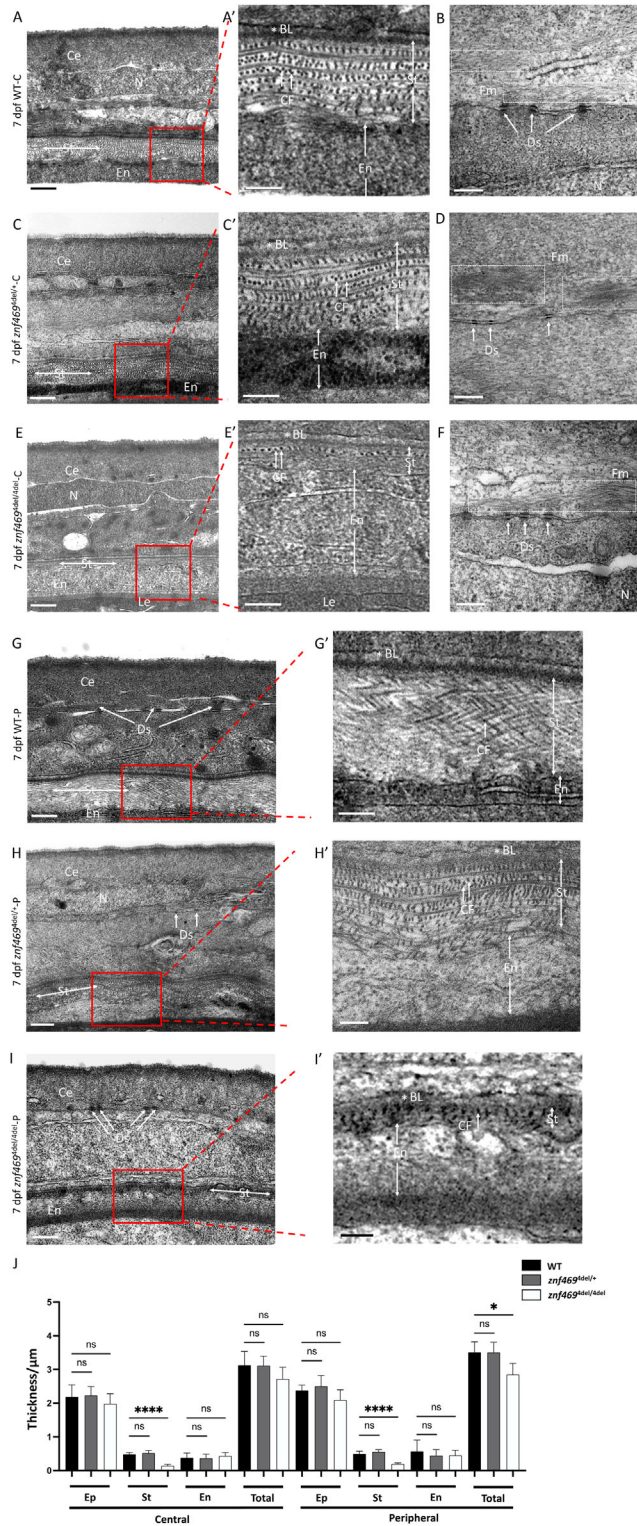


**FIGURE 6.** *znf469* homozygous mutation in zebrafish results in a significant reduction of corneal stroma thickness at 7 dpf. TEM ultrastructure of the cornea is shown in WT (A, A', B, G, G'), *znf469*<sup>4del/+</sup> (C, C', D, H, H'), and *znf469*<sup>4del/4del</sup> (E, E', F, I, I') zebrafish larvae at 7 dpf. The stroma components decreased significantly, and only a few orderly arranged collagen fiber lamellae can be seen in *znf469*<sup>4del/4del</sup> mutant zebrafish at 7 dpf. A, C, and E show the central cornea at low magnification. G, H, and I show the peripheral cornea at low magnification. A', C', E', G', H', and I' are the enlarged images of the primary stroma shown in the red boxes in A, C, E, G, H, and I, respectively; B, D, and F show that fibril-

like materials and cell junctions (desmosomes) could be observed in *znf469*<sup>4del/+</sup> and *znf469*<sup>4del/4del</sup> zebrafish at 72 hpf, with no significant difference compared to WT zebrafish. J shows the thickness of each layer of the total, central, and peripheral cornea in WT, *znf469*<sup>4del/+</sup>, and *znf469*<sup>4del/4del</sup> zebrafish at 7 dpf. The thickness of the central and peripheral stroma is significantly reduced in the *znf469*<sup>4del/4del</sup> mutant ( $n = 5$  for each genotype; data are shown as the mean  $\pm$  SD; \* $P < 0.05$ , \*\*\*\* $P < 0.0001$ ). Ce, corneal epithelium; N, nucleus; St, stroma; En, endothelium; Le, lens epithelium; R, retina; BL, Bowman's layer; CF, collagen fiber; Fm, fibril-like material; Ds, desmosome. Scale bars: 500 nm (A, C, E, G, H, I, D); 200 nm (A', C', E', G', H', I', B, D).

was extremely reduced compared to that of WT zebrafish at 72 hpf, and collagen fibers were barely observed and disorganized in both the central and the peripheral cornea (Figs. 5E, 5E', 5I, 5I'). The other shapes and structures of the cornea were similar to those of the WT larvae, with a fibril-like structure, and the desmosomes (Figs. 5F, 5I). For *znf469*<sup>4del/+</sup> zebrafish at 72 hpf, no difference was observed in the corneal structure or the thickness of each layer compared to WT zebrafish (Figs. 5C, 5C', 5D, 5H, 5H'). We measured the thickness of the total cornea and each layer of the cornea and found that, as the TEM photographs reveal, the stromal thickness of *znf469*<sup>4del/4del</sup> mutant zebrafish was extremely reduced compared to that of WT zebrafish (central:  $0.1942 \pm 0.02607 \mu\text{m}$  vs.  $0.5628 \pm 0.08867 \mu\text{m}$ ,  $P < 0.0001$ ; peripheral:  $0.2448 \pm 0.0513 \mu\text{m}$  vs.  $0.6668 \pm 0.1200 \mu\text{m}$ ,  $P < 0.0001$ ). In addition, we found that the central corneal thickness of *znf469*<sup>4del/4del</sup> zebrafish was thinner than that of WT zebrafish ( $5.215 \pm 0.2018 \mu\text{m}$  vs.  $5.769 \pm 0.4282 \mu\text{m}$ ;  $P = 0.0309$ ) (Fig. 5J). For the other ocular tissues, such as retina and lens, it seems that the mutation of *znf469* did not affect their morphogenesis during zebrafish development (Supplementary Fig. S1).

The WT cornea at 7 dpf was similar to that observed at 72 hpf which contained two layers of epithelial cells: a stromal layer and a monolayer of endothelium. However, the epithelial cells become flattened, and the thickness of the epithelium was reduced by approximately a half comparing to that at 72 hpf (Figs. 6A, 6G). Although the stromal layer continued to grow slightly, the thickness of the stroma changed very little between 72 hpf and 7 dpf. However, the stroma was arranged in a more orderly manner (Figs. 6A, 6A', 6G, 6G'). For *znf469*<sup>4del/4del</sup> zebrafish at 7 dpf, the thickness of the stroma was also extremely reduced compared to that of WT zebrafish at 7 dpf; only a few disorganized collagen fibers were observed below Bowman's layer in the central and peripheral cornea (Figs. 6E, 6E', 6I, 6I', 6J). Otherwise, the shape and cellular structure of the cornea were similar to those of the WT cornea, and the desmosomes still existed (Figs. 6F, 6I). For *znf469*<sup>4del/+</sup> zebrafish at 7 dpf, no significant difference was observed in the corneal structure or the thickness of each layer compared to WT zebrafish (Figs. 6C, 6C', 6D, 6H, 6H', 6J). Expectedly, the corneal stroma of *znf469*<sup>4del/+</sup> adult zebrafish seemed to be unaffected compared to that of WT zebrafish (Supplementary Fig. S2). Unfortunately, due the lethality of *znf469*<sup>4del/4del</sup> mutation in zebrafish, we could not investigate the phenotype in elder or adult homozygous mutant zebrafish. The above results suggest that *znf469* is essential for the formation of the primary stroma during corneal development in zebrafish.

like materials and cell junctions (desmosomes) could be observed in *znf469*<sup>4del/+</sup> and *znf469*<sup>4del/4del</sup> zebrafish at 72 hpf, with no significant difference compared to WT zebrafish. J shows the thickness of each layer of the total, central, and peripheral cornea in WT, *znf469*<sup>4del/+</sup>, and *znf469*<sup>4del/4del</sup> zebrafish at 7 dpf. The thickness of the central and peripheral stroma is significantly reduced in the *znf469*<sup>4del/4del</sup> mutant ( $n = 5$  for each genotype; data are shown as the mean  $\pm$  SD; \* $P < 0.05$ , \*\*\*\* $P < 0.0001$ ). Ce, corneal epithelium; N, nucleus; St, stroma; En, endothelium; Le, lens epithelium; R, retina; BL, Bowman's layer; CF, collagen fiber; Fm, fibril-like material; Ds, desmosome. Scale bars: 500 nm (A, C, E, G, H, I, D); 200 nm (A', C', E', G', H', I', B, D).





proteasome pathway, the ECM-receptor interaction pathway, and the cell cycle pathway (Fig. 7C). Interestingly, 35 genes enriched in the proteasome pathway were all upregulated, and 19 and 23 genes enriched in the ECM-receptor pathway and cell cycle pathway, respectively, were all downregulated. The identified genes by RNA-seq were partially confirmed by qRT-PCR experiments (Fig. 7D). In summary, our data indicate that, widely considered as a transcription factor, *znf469* might target a great number of ECM-related genes, including virtually all collagen and proteasome genes, to regulate the synthesis and homeostasis of ECM, thus affecting development of the corneal stroma.

## DISCUSSION

In this study, we demonstrated the ocular features of a patient with *ZNF469* mutation and then we generated a *znf469*<sup>4del/4del</sup> zebrafish model of BCS using CRISPR/Cas9 technology. The model reproduced the phenotypic ocular features caused by *ZNF469* mutations. Deletion of *znf469* led to a severe reduction in the stroma in the total cornea in zebrafish larvae from the early developmental stage (3 dpf), which is similar to the situation in which keratoconus in BCS usually appears during adolescence, even 6-week-old patients.<sup>23</sup> RNA-seq analysis revealed that the synthesis and degradation of a large number of ECM components, such as collagens and proteoglycans, as well as the 26S proteasome family members, are affected.

There are both positive and negative reports on whether *ZNF469* heterozygous missense mutations are related to KC.<sup>11–15</sup> These conflicts may be due to the difficulty of assessing the impact of missense mutations on such a poorly characterized protein in silico and the different regions and races. The patient reported in this study developed KC in BCS. In the zebrafish model, *znf469*<sup>4del/+</sup> zebrafish did not display an apparent phenotype in cornea or other tissues, which is consistent with the observation in mice.<sup>18</sup> This observation suggests that *znf469* may have varied roles in different species or that the heterozygous missense mutations in humans bring about gain-of-function or dominant-negative effects.<sup>14</sup> Different from in mice and humans, depletion of *Znf469* is lethal and induces more severe disorder in corneal stroma in zebrafish, suggesting that it may play more important roles in zebrafish. We observed only the sharp decrease in the thickness of the corneal stroma, but not in total corneal thickness. It should be because the stroma accounts for 90% of the human cornea (approximately 500  $\mu$ m),<sup>24</sup> but in zebrafish at 3 to 7 dpf and adults, the percentages are only 10% to 15% and 30% to 40%, respectively,<sup>20,25</sup> and the depletion of *Znf469* did not affect the structure of the corneal epithelia and endothelia. Unfortunately, the lethality of *znf469*<sup>4del/4del</sup> in zebrafish larvae prevented us from exploring the longer course of the disease in this model. Notably, the cellular origin and composition of the corneal stroma under study here are those of the primary stroma, not the same as the thin stroma apparent in BCS, although it may be a precursor to it.

At the molecular level, our data suggest that many more downstream candidates than current known may be affected by depletion of *Znf469*. Collagen I is the major component of the corneal stroma in vertebrates and is encoded by *COL1A1* and *COL1A2*.<sup>26</sup> Consistent with in mice, reduced *col1a1a* was observed in *znf469*<sup>4del/4del</sup> zebrafish mutants. We also observed a noninflated swimbladder in the mutants, resembling the *col1a1a*<sup>-/-</sup> zebrafish model.<sup>27</sup> Primary kera-

toocyte cultures taken from the *Zfp469*<sup>BCS/BCS</sup> mouse indicate the significantly decreased synthesis of *Col1a1* and *Col1a2* but not *Col5a1*.<sup>18</sup> In zebrafish, it seems that depletion of *Znf469* affects the expression of most of collagen, such as *col1a1a*, *col1a1b*, *col1a2*, *col2a1a*, *col2a1b*, *col5a1*, and *col5a3b*. *PRDM5* (PR/SET domain 5) is considered to act on a common pathway regulating ECM gene expression.<sup>1,28</sup> As a transcriptional regulator, *Prdm5* targets all mouse collagen genes and some other proteoglycan genes. Moreover, *Prdm5* sustains the transcription of collagen I genes by binding RNA polymerase II,<sup>29</sup> which closely resembles our results. We infer that *znf469* may comparably target a large number of ECM component genes and regulates their transcription.

An additional interesting result is the overall upregulation of proteasome family members and other regulators in *znf469*<sup>4del/4del</sup> mutant zebrafish. Supporting this observation, a proteomic study of KC indicated that ubiquitin proteasomal degradation pathway members were elevated.<sup>30</sup> A patient with *ZNF469* mutation showed increased urinary pyridinoline (PYR) and deoxypyridinoline (DPYR) concentrations and an elevated DPYR/PYR ratio,<sup>31</sup> suggesting complicated downstream targets of *ZNF469*. Although we cannot exclude the possibility that the proteasome genes were upregulated due to the misfolding of the truncated *Znf469* protein, we infer that *ZNF469* may regulate the transcription of 26S proteasome family members, thereby promoting the degradation of ECM. Together with the reduced synthesis of ECM components, *ZNF469* mutations ultimately result in all of the phenotypes. Further experiments such as chromatin immunoprecipitation followed by sequencing should be performed to clarify its roles as a considered transcription factor and the downstream candidates of *Znf469*. Furthermore, the RNA-seq data reported in this study were obtained from whole embryos; tissue-specific sample preparations for RNA-seq would be beneficial for obtaining insight into BCS.

In summary, this study suggests that *znf469* is a critical gene that may regulate the synthesis and degradation of a large number of ECM components and is closely related to the formation of BCS.

## Acknowledgments

The authors thank the Bio-Ultrastructure Analysis Lab of the Analysis Center of Agrobiology and Environmental Sciences, Zhejiang University, for TEM assistance.

Supported by grants from the Program of National Natural Science Foundation of China (82171033 and 81970781 to XS) and the Natural Science Foundation of Zhejiang Province (LD21H120001 to XS).

Disclosure: **J. Bao**, None; **X. Yu**, None; **X. Ping**, None; **X. Shentu**, None; **J. Zou**, None

## References

- Burkitt Wright EM, Porter LF, Spencer HL, et al. Brittle cornea syndrome: recognition, molecular diagnosis and management. *Orphanet J Rare Dis*. 2013;8:68.
- Dhooge T, Van Damme T, Syx D, et al. More than meets the eye: expanding and reviewing the clinical and mutational spectrum of brittle cornea syndrome. *Human Mutation*. 2021;42:711–730.
- Tadepally HD, Burger G, Aubry M. Evolution of C2H2-zinc finger genes and subfamilies in mammals: species-specific duplication and loss of clusters, genes and effector domains. *BMC Evol Biol*. 2008;8:176.

4. Lu Y, Dimasi DP, Hysi PG, et al. Common genetic variants near the Brittle Cornea Syndrome locus *ZNF469* influence the blinding disease risk factor central corneal thickness. *PLoS Genet.* 2010;6:e1000947.
5. Vitart V, Bencic G, Hayward C, et al. New loci associated with central cornea thickness include *COL5A1*, *AKAP13* and *AVGR8*. *Hum Mol Genet.* 2010;19:4304–4311.
6. Vithana EN, Aung T, Khor CC, et al. Collagen-related genes influence the glaucoma risk factor, central corneal thickness. *Hum Mol Genet.* 2011;20:649–658.
7. Hoehn R, Zeller T, Verhoeven VJ, et al. Population-based meta-analysis in Caucasians confirms association with *COL5A1* and *ZNF469* but not *COL8A2* with central corneal thickness. *Hum Genet.* 2012;131:1783–1793.
8. Gao X, Gauderman WJ, Liu Y, et al. A genome-wide association study of central corneal thickness in Latinos. *Invest Ophthalmol Vis Sci.* 2013;54:2435–2443.
9. Vincent AL, Jordan CA, Cadzow MJ, Merriman TR, McGhee CN. Mutations in the zinc finger protein gene, *ZNF469*, contribute to the pathogenesis of keratoconus. *Invest Ophthalmol Vis Sci.* 2014;55:5629–5635.
10. Gao X, Nannini DR, Corrao K, et al. Genome-wide association study identifies *WNT7B* as a novel locus for central corneal thickness in Latinos. *Hum Mol Genet.* 2016;25:5035–5045.
11. Yildiz E, Bardak H, Gunay M, et al. Novel zinc finger protein gene 469 (*ZNF469*) variants in advanced keratoconus. *Curr Eye Res.* 2017;42:1396–1400.
12. Yu X, Chen B, Zhang X, Shentu X. Identification of seven novel *ZNF469* mutations in keratoconus patients in a Han Chinese population. *Mol Vis.* 2017;23:296–305.
13. Zhang W, Margines JB, Jacobs DS, et al. Corneal perforation after corneal cross-linking in keratoconus associated with potentially pathogenic *ZNF469* mutations. *Cornea.* 2019;38:1033–1039.
14. Davidson AE, Borasio E, Liskova P, et al. Brittle cornea syndrome *ZNF469* mutation carrier phenotype and segregation analysis of rare *ZNF469* variants in familial keratoconus. *Invest Ophthalmol Vis Sci.* 2015;56:578–586.
15. Karolak JA, Gambin T, Rydzanicz M, et al. Evidence against *ZNF469* being causative for keratoconus in Polish patients. *Acta Ophthalmol.* 2016;94:289–294.
16. Rohrbach M, Spencer HL, Porter LF, et al. *ZNF469* frequently mutated in the brittle cornea syndrome (BCS) is a single exon gene possibly regulating the expression of several extracellular matrix components. *Mol Genet Metab.* 2013;109:289–295.
17. Abu A, Frydman M, Marek D, et al. Deleterious mutations in the Zinc-Finger 469 gene cause brittle cornea syndrome. *Am J Hum Genet.* 2008;82:1217–1222.
18. Stanton CM, Findlay AS, Drake C, et al. A mouse model of brittle cornea syndrome caused by mutation in *Zfp469*. *Dis Model Mech.* 2021;14:dmm049175.
19. Ping X, Liang J, Shi K, et al. Rapamycin relieves the cataract caused by ablation of *Gja8b* through stimulating autophagy in zebrafish. *Autophagy.* 2021;17:3323–3337.
20. Zhao XC, Yee RW, Norcom E, et al. The zebrafish cornea: structure and development. *Invest Ophthalmol Vis Sci.* 2006;47:4341–4348.
21. Bibliowicz J, Tittle RK, Gross JM. Toward a better understanding of human eye disease insights from the zebrafish, *Danio rerio*. *Prog Mol Biol Transl Sci.* 2011;100:287–330.
22. Greiling TM, Clark JI. Early lens development in the zebrafish: a three-dimensional time-lapse analysis. *Dev Dyn.* 2009;238:2254–2265.
23. Ramappa M, Wilson ME, Rogers RC, Trivedi RH. Brittle cornea syndrome: a case report and comparison with Ehlers Danlos syndrome. *J AAPOS.* 2014;18:509–511.
24. Espana EM, Birk DE. Composition, structure and function of the corneal stroma. *Exp Eye Res.* 2020;198:108137.
25. Akhtar S, Schonhaler HB, Bron AJ, Dahm R. Formation of stromal collagen fibrils and proteoglycans in the developing zebrafish cornea. *Acta Ophthalmol.* 2008;86:655–665.
26. Ihanamaki T, Pelliniemi LJ, Vuorio E. Collagens and collagen-related matrix components in the human and mouse eye. *Prog Retin Eye Res.* 2004;23:403–434.
27. Gistelinc C, Kwon RY, Malfait F, et al. Zebrafish type I collagen mutants faithfully recapitulate human type I collagenopathies. *Proc Natl Acad Sci USA.* 2018;115:E8037–E8046.
28. Burkitt Wright EMM, Spencer HL, Daly SB, et al. Mutations in *PRDM5* in brittle cornea syndrome identify a pathway regulating extracellular matrix development and maintenance. *Am J Hum Genet.* 2011;88:767–777.
29. Galli GG, Honnens de Lichtenberg K, Carrara M, et al. *Prdm5* regulates collagen gene transcription by association with RNA polymerase II in developing bone. *PLoS Genet.* 2012;8:e1002711.
30. Shinde V, Hu N, Renuse S, et al. Mapping keratoconus molecular substrates by multiplexed high-resolution proteomics of unpooled corneas. *OMICS.* 2019;23:583–597.
31. Al-Owain M, Al-Dosari MS, Sunker A, Shuaib T, Alkuraya FS. Identification of a novel *ZNF469* mutation in a large family with Ehlers–Danlos phenotype. *Gene.* 2012;511:447–450.